J Mater Sci (2013) 48:1465–1473
DOI 10.1007/s10853-012-6900-6

Effect of annealing atmosphere (Ar vs. air) and temperature on the electrical and optical properties of spin-coated colloidal indium tin oxide films

Salil M. Joshi · Rosario A. Gerhardt

Received: 27 May 2012 / Accepted: 15 September 2012 / Published online: 28 September 2012

Abstract Colloidal indium tin oxide (ITO) ~6 nm nanoparticles synthesized in-house were deposited by spin coating on fused silica substrates, resulting in high resistivity films due to the presence of passivating organics. These films were annealed at various temperatures ranging from 150 to 750 °C in air and argon atmospheres. The films are very transparent in the as-coated form, and they retain high transparency upon annealing, except the films annealed at 300 °C in argon, which became brown due to incomplete pyrolysis of the organics. Thermogravimetric analysis and Raman characterization showed that the removal of organics increases with an increase in the annealing temperature, and that this removal is more efficient in the oxidizing atmosphere of air, especially in the 300–450 °C temperature range than in Ar. Although ITO defect chemistry suggests that argon annealing should result in higher carrier concentration than air annealing, the faster removal of insulating organics upon annealing in air resulted in significantly lower film resistivity at intermediate annealing temperatures for films annealed in air than in Ar. At higher annealing temperatures, both Ar and air annealing, resulted in comparable film resistivities (the lowest achieved was $\sim 10^0$ Ω cm).

Electronic supplementary material The online version of this article (doi:10.1007/s10853-012-6900-6) contains supplementary material, which is available to authorized users.

S. M. Joshi · R. A. Gerhardt (✉)
School of Materials Science and Engineering, Georgia Institute of Technology, Atlanta, GA, USA
e-mail: rosario.gerhardt@mse.gatech.edu

Introduction

Transparent conductors find important applications in many different optoelectronic devices such as photovoltaic cells, LED displays, and others. Indium Tin oxide (ITO) is perhaps the most widely used transparent conductor. ITO is highly transparent in the visible region on account of its large band gap [1], with near metallic conductivity as a result of conduction electrons generated through tin doping, which causes oxygen vacancies and generates charge carriers (mobile electrons) [2]. Zinc oxide-based transparent conductors such as aluminum-doped zinc oxide (AZO) are also used in similar applications as ITO because they have similar levels of transparency and electrical conductivity [3]. However, they have been found to be more susceptible to moisture and atmospheric degradation [4]. Current commercial fabrication techniques for ITO coatings involve vacuum techniques such as RF magnetron sputtering and electron beam evaporation [5, 6]. In addition to the expensive equipment required, the material that is wasted during deposition [7, 8] the need for a heated substrate to achieve optimum properties [9, 10] makes vapor deposition methods unsuitable for depositing ITO patterned circuits onto flexible and heat sensitive polymer substrates.

The need for flexible displays and transparent conductors for organic photovoltaic cells and other flexible optoelectronic devices makes it imperative that methods to fabricate good quality transparent conducting coatings with minimal heat treatment be developed. Direct fabrication of transparent conducting films and circuits from "inks" made from colloidal, crystalline ITO nanoparticles, or other transparent conductive materials may be the basis for developing processes that minimize ITO waste, and may be used with heat sensitive flexible substrates. Some progress has been made in this area but the method used to

synthesize ITO nanoparticles, and deposit the films and patterns fabricated from them may need further processing to various extents in order to obtain the required properties for each application [11–13].

The ITO nanoparticles used for this study were synthesized following a method developed in-house [14]. An earlier paper [15] on spin-coated colloidal films presented an overview of the effect of plasma treatment and annealing in air on the dc resistivity of colloidal ITO films using these nanoparticles. In that paper [15], XPS data was used to detect the change in the carbon 1s peaks as the air annealing temperature was varied. Some data comparing two different plasma treatments was also provided; however, no data corresponding to argon (Ar) annealing of colloidal films was included. In contrast, this study compares the effect of Ar and air atmospheres on the electrical and optical properties of spin-coated colloidal thin films annealed at different temperatures.

The ITO nanoparticles used in this study were sterically stabilized in non-polar solvents like hexane, due to the presence of stabilizing myristic acid ligands on the surface of the nanoparticles [14]. This is schematically illustrated in Fig. 1, which shows a cartoon of ITO nanoparticles surrounded by myristic acid ligands. Although the ITO nanoparticles themselves are good electron conductors, the passivating ligands on their surface and inter-particle porosity result in poor electrical contacts between the nanoparticles when they are deposited in the form of a film. As a result, carrier transport between the nanoparticles is impeded, and as reported previously [15], the as-coated films of colloidal ITO have very high resistivity ($\sim 10^8$ Ω cm). The electrical properties of the films may be improved by removing the residual organics and reducing the porosity. The residual organics may be removed by post-processing treatments, such as annealing at a high temperature in air (organics removal by oxidation) or in an inert atmosphere (organics removal by pyrolysis), or by plasma treatment (reactive ion etching) [16], or by liquid phase/solution-based etching.

In this paper, crucial thermogravimetric data and Raman spectra are used to show the differences in the efficiency of ligand removal in air as compared to Ar. However, as will be described later in the paper, annealing treatments alone cannot improve the electrical conductivity of the films at temperatures low enough to be useful for applications on heat sensitive, flexible substrates but the data presented here will be shown to be very useful in future publications.

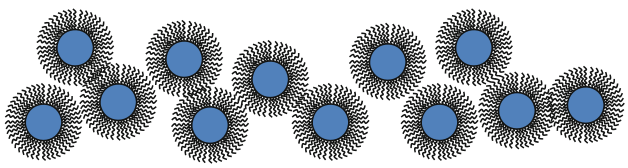

Fig. 1 Schematic representation of sterically stabilized ITO nanoparticles

Experimental details

Colloidal ITO nanoparticles, with tin content equivalent to 18 wt% SnO_2 were synthesized by a non-aqueous technique using indium and tin acetate salts as precursors, myristic acid and 1-octadecanol in a high boiling point, non-polar solvent, 1-octadecene as described earlier [15]. The ITO nanoparticles were precipitated using standard polar/non-polar solvent techniques [17] and dispersed in hexane. This dispersion of colloidal ITO nanoparticles was spin coated onto 12.7×12.7 mm^2 ($0.5'' \times 0.5''$)-fused silica substrates and resulted in films that were approximately 200 nm thick. More details about the synthesis and film fabrication by spin coating are described elsewhere [15]. The films reported in this paper were annealed at various temperatures: 150, 300, 450, 600, and 750 °C in UHP grade commercial air and UHP grade Ar. This was done in a controlled atmosphere alumina tube furnace with a ramp up rate of 3 °C/min.

The optical transmittance of the films was characterized by UV–visible absorption spectroscopy on a Cary 5000 spectrophotometer, using a clean uncoated fused quartz substrate as the baseline. The percent transmittance in the visible region was calculated by taking the average of the transmittance over the wavelength window of 400–700 nm. The electrical characterization of the colloidal ITO films was done by impedance spectroscopy (IS). This technique provides a wealth of additional information not accessible from dc measurements alone, because in IS, the electrical response is collected as a function of frequency. Measurements were performed using a four-point probe set-up with 62.5 mils (1.5875 mm) tip spacing and a tip radius of 1.6 mils (40.64 μm). The equipment used was a Solartron 1260 Impedance Analyzer in conjunction with a Solartron 1296 dielectric interface at frequencies ranging from 0.1 Hz to 1 MHz. This set-up allowed us to make many measurements on each of the $0.5'' \times 0.5''$ film samples at different locations on the film. Measurements were averaged from a minimum of five scans and the standard deviations are shown as error bars in the resistivity plots presented in the paper.

The effect of heating on the degradation of residual organics in the dried colloidal ITO was analyzed by thermogravimetric analysis (TGA). This was done in UHP Ar and commercial air atmospheres. In order to circumvent the difficulty of determining an accurate initial weight due to the non-trivial rate of evaporation of the hexane solvent in ambient conditions, the TGA sample pan was filled with

ITO solution and dried by placing on a controlled temperature hot plate maintained at approximately 90 °C. TGA was done on a Q50 thermogravimetric analyzer from TA Instruments, using a sample purge gas flow of 10 mL/min and a temperature ramp rate of 5 °C/min up to a temperature of 750 °C. In addition, Raman spectroscopy was done on selected colloidal ITO films to get further insights into the degradation of the residual organics. Films annealed at 300 and 600 °C, in addition to as-coated films and an uncoated fused silica substrate were chosen for Raman spectroscopy measurements. Annealing temperatures of 300 and 600 °C were chosen because TGA and other characterization techniques indicated partial and near complete degradation of the residual organics at these temperatures, respectively. Raman spectroscopy was carried out on a Thermo Scientific DXR Raman microscope, using a laser of wavelength 532 nm. Since the films annealed in air and Ar were characterized in separate batches, Raman spectroscopy of the as-coated film was repeated to ascertain reproducibility.

Results

Optical properties

The as-synthesized ITO nanoparticles were spheroidal in shape, and had a narrow size distribution of about 6 nm diameter. TEM images of similarly prepared ITO nanoparticles were presented in previous publications [14, 15]. Figure 2 shows the visual appearance of the coated films in the as-coated condition as well as after annealing at various temperatures from 150 to 450 °C in Ar and in air. It can be seen that the as-deposited films are very transparent, and stay transparent after most annealing treatments, except for the film annealed at 300 °C in Ar, which shows noticeable darkening. Figure 3a, b depicts representative scans of the percent transmittance of films over the visible spectrum for ITO films annealed at different temperatures in Ar and in air, respectively. Most of the ITO films are very transparent through the visible region, and a small decrease in transmittance can be observed at the blue-UV end of the spectrum, which starts approaching the optical band gap of ITO. The film annealed at 300 °C in Ar, absorbed significantly in the visible region, corresponding to its dark appearance.

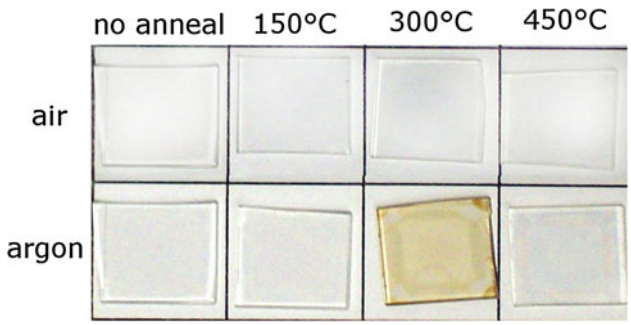

Fig. 2 Visual appearance of colloidal ITO films as a result of annealing at different temperatures in air and in Ar. The size of substrates used is approximately 12.7 x 12.7 mm^2 (0.5 x 0.5 in)

Figure 4 displays the percent optical transmittance averaged over the visible wavelengths (400–700 nm) for the films, as a function of annealing temperature and atmosphere. Although the optical transmittance in the visible region is high in the as-coated colloidal ITO films, as well as after most of the annealing treatments, the average optical transmittance in the visible region was significantly reduced in the colloidal ITO film annealed at 300 °C in Ar, and to a less extent in the colloidal ITO film annealed at 450 °C in Ar. This may be attributed to the incomplete pyrolysis of the organics, which resulted in charring of the organics, which was manifested particularly in the 300 °C, Ar-annealed film as a darker, brown colored film.

Thermal analysis and Raman spectroscopy

The percent weight loss of dried colloidal ITO, as determined by the thermogravimetric analysis, is shown in Fig. 5a; and the corresponding rate of weight loss is shown in Fig. 5b for both air and Ar. The weight loss can primarily be correlated to the degradation and removal of any residual solvent and organics from the colloidal ITO. At temperatures greater than 150 °C, the weight loss in air is observed to be significantly higher than the corresponding weight loss on heating in Ar. The weight loss in air seems to occur in a single step, with the maximum rate of weight loss at around 348.5 °C, leading to a total maximum weight loss of about 30 %. The weight loss upon heating in air seems to reach completion at temperatures between 350 and 400 °C. The weight loss upon heating in Ar seems to reach completion at temperatures around 750 °C. The slight uptick in the weight corresponding to a little more than 1 %, seen at temperatures above 600 °C in either atmosphere, could very likely be the result of an instrument error at those temperatures. Although the total maximum weight loss on heating in Ar is approximately identical to that in air, around 30 %; Fig. 5b shows that it occurs in two stages, with peak rate of weight loss at 408.44 and 497.49 °C, respectively. From this TGA data, we can conclude that the degree of organics removal may be expected to be higher in films annealed in air as compared to those annealed at the same temperature in Ar, even for colloidal ITO films annealed at temperatures as high as 450 °C.

In order to get a measure of the organics present in the ITO film at different stages of the annealing heat treatments,

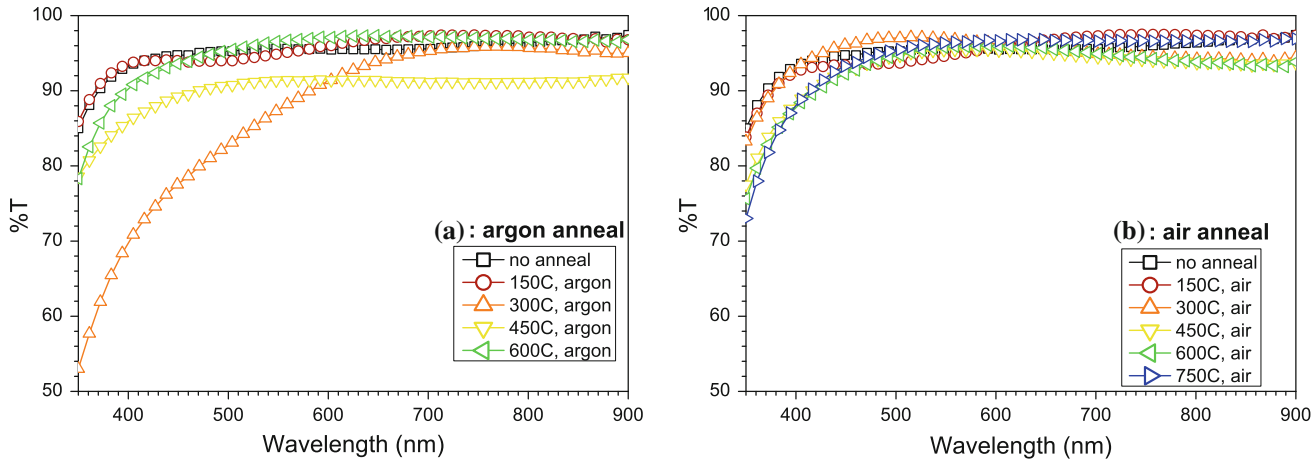

Fig. 3 Variation of percent transmittance over the visible spectrum of colloidal ITO films for different annealing temperatures in air and in Ar

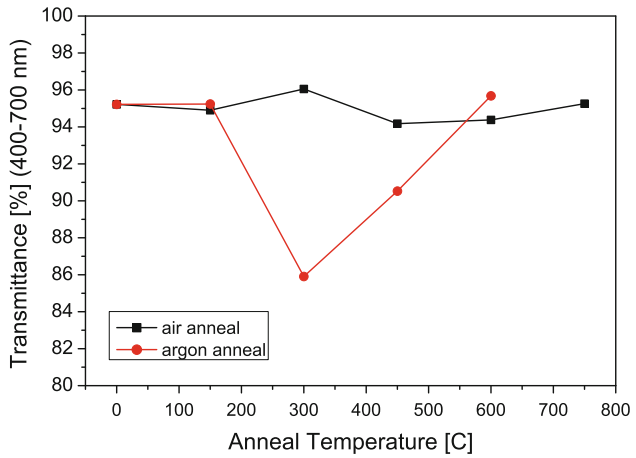

Fig. 4 Average optical transmittance of colloidal ITO films in the visible region (400–700 nm) as a function of annealing conditions

Raman spectroscopy experiments were conducted. Figure 6a, b shows a comparison of Raman spectra of the as-coated colloidal ITO films with the spectrum of an uncoated substrate (fused silica), as well as spectra of the various organic reagents and solvents (tin acetate, indium acetate, 1-octadecene, hexane, myristic acid) that were used in the synthesis of the colloidal ITO solution, and could be potentially present in small amounts. The spectra of the organic compounds were obtained in image or pdf format from the spectral database for organic compounds SDBS [18], maintained by the National Institute of Advanced Industrial Science and Technology (AIST), Japan, and product Raman spectra from Sigma Aldrich Chemical Company [19]. These were converted to digital form using an open source software, Plot Digitizer [20]. The smaller Raman shifts, below 1100 $\Omega\ cm^{-1}$ are dominated by

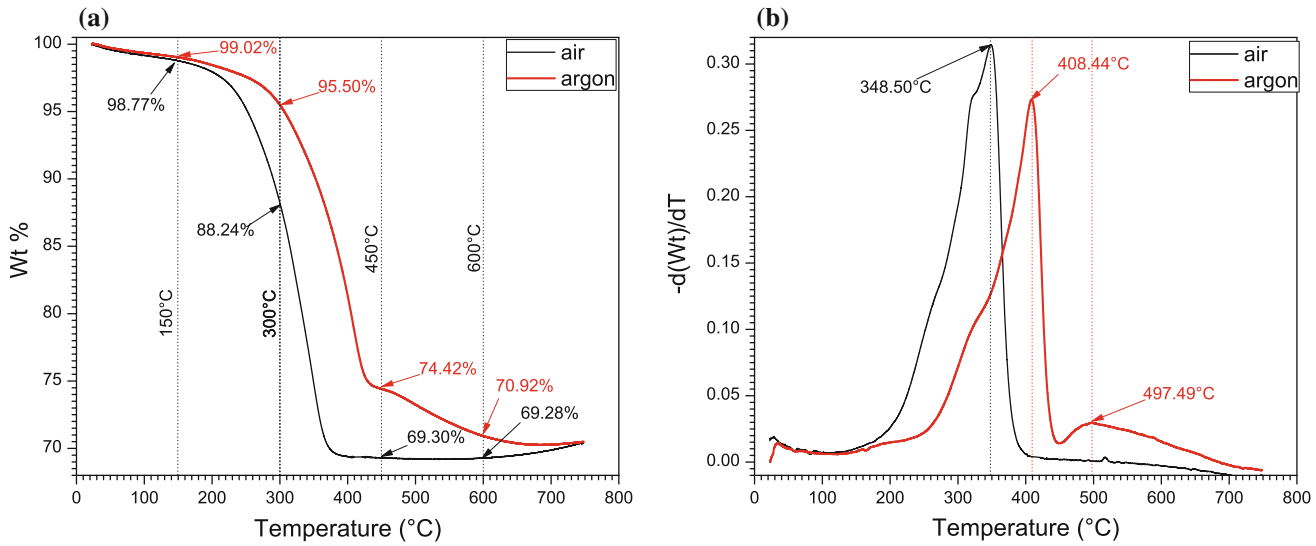

Fig. 5 Thermogravimetric analysis (TGA) on colloidal ITO after solvent removal at 90 °C: **a** percent change in weight with temperature, **b** derivative of weight change with temperature

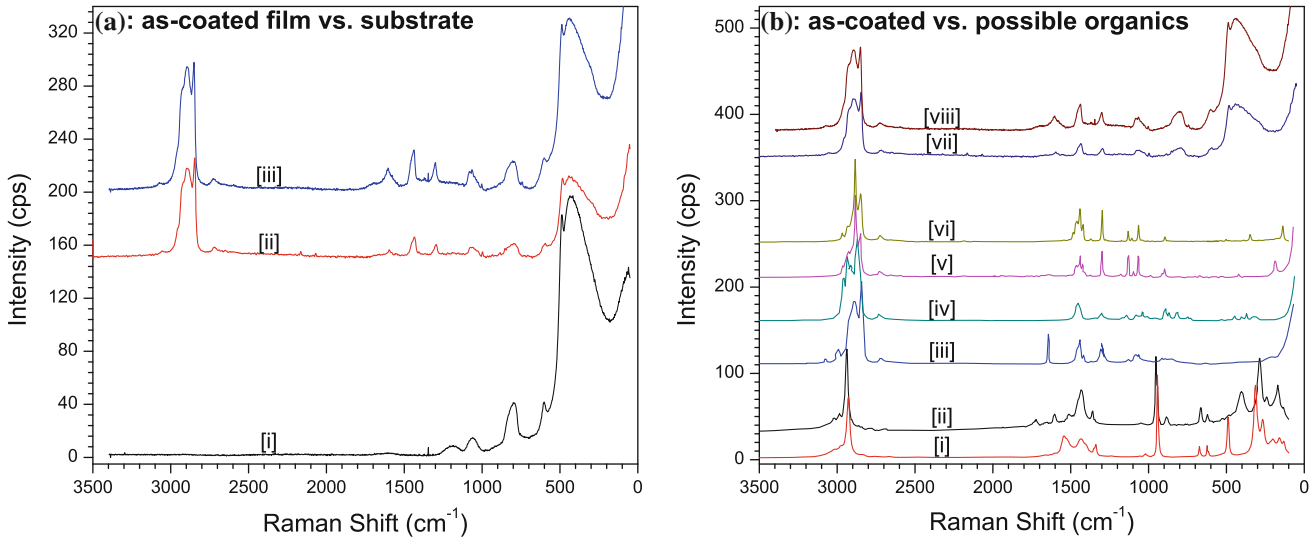

Fig. 6 Comparison of Raman spectra of non-annealed colloidal ITO films with **a** substrate, **b** possible organic compounds present residually in the as-prepared colloidal ITO solution spectra in (**a**) are : (*i*) fused silica substrate, (*ii*) non-annealed 1, (*iii*) non-annealed 2. Spectra in (**b**) are: (*i*) tin acetate, (*ii*) indium acetate hydrate, (*iii*) 1-octadecene, (*iv*) hexane, (*v*) myristic acid, (*vi*) 1-octadecanol, (*vii*) as-coated-1, (*viii*) as-coated-2

scattering from the fused silica substrate, and what appears to be Rayleigh scattering that was not completely filtered out. The peaks in the 2800–3000 cm^{-1} correspond to scattering from the $–CH_2$ and $–CH_3$ bonds [21]; and are common to most organic compounds. These peaks are prominent in the Raman spectra of the as-coated films. Myristic acid is not only expected to be present as passivating ligands on the surface of the nanoparticles, but also in the form of some excess free myristic acid that could not be completely removed during extraction. The spectra indicate possible peaks from 1-octadecene, which was used during the synthesis [14, 15] as a high boiling point, non-polar solvent. It was subsequently removed by precipitating the nanoparticles using standard polar/non-polar solvent techniques [17]. However, the presence of Raman peaks indicates that perhaps some residual 1-octadecene may have persisted. This is significant because 1-octadecene has a boiling point of 315 °C [22]; and the residual amounts of 1-octadecene would not have been able to be removed by lower temperature treatments.

Figure 7a, b presents Raman spectra for films annealed at 300 and 600 °C in air and Ar, respectively, and compares them with the spectra of an as-coated colloidal ITO film. It can be seen that the peaks corresponding to $–CH_2$

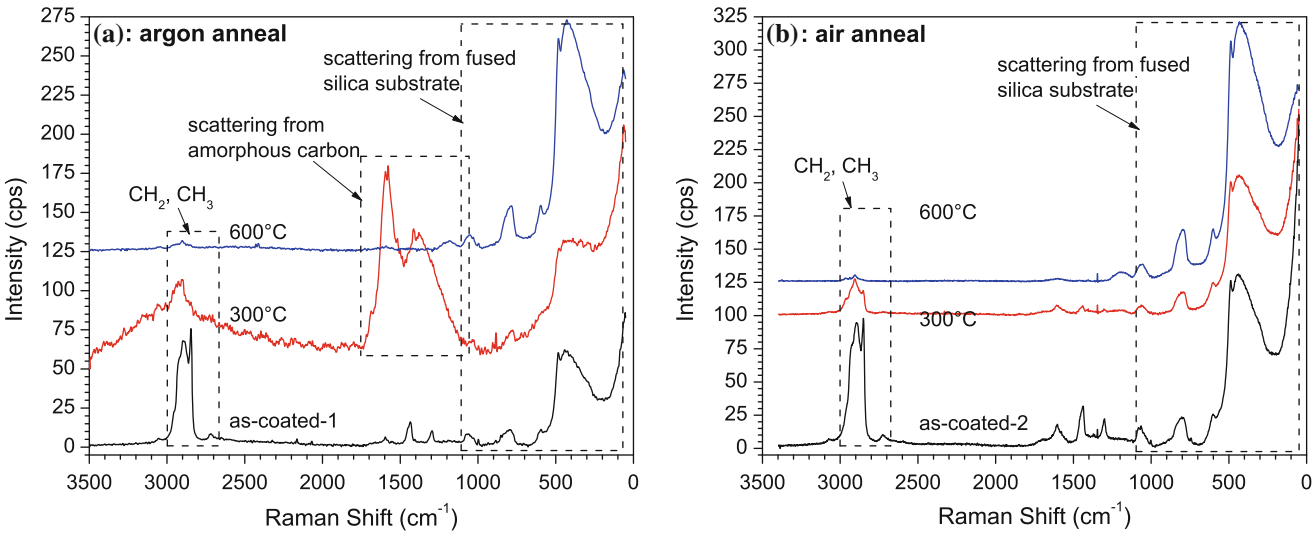

Fig. 7 Comparison of Raman spectra of as-coated colloidal ITO films with those of **a** ITO films annealed in Ar at 300 and 600 °C, **b** ITO films annealed in air at 300 and 600 °C

and $-CH_3$ progressively decrease with an increase in annealing temperature. The Raman spectra of films annealed at 300 °C in air and in Ar show a stark difference. The film annealed in air displays significantly lower signals from organics as compared to the film annealed in Ar. For the film annealed in Ar, it not only shows a broad peak in the 2800–3200 cm^{-1} range, which corresponds to $-CH_2$ and $-CH_3$, but also broad peaks in the 1200–1800 cm^{-1} range, which indicates the presence of amorphous carbon [23, 24]. In contrast, the Raman spectra of films annealed in either atmosphere at 600 °C appear very similar. Apart from very faint scattering signal from CH_2– and CH_3– present in both, the Raman spectra show very little signal from any organics. Instead, these spectra are dominated by scattering from the fused silica substrate, which appears below 1000 cm^{-1}. These results corroborate the conclusions from the TGA data that upon heating to 600 °C and beyond in either air or in Ar, most of the residual organics have been removed.

Electrical properties

As described earlier, impedance spectroscopy was used to measure the electrical response of the ITO thin films. Representative Bode plots depicting the variation of impedance magnitude and the impedance phase angle are shown in Fig. 8 for colloidal ITO films annealed at various temperatures in air (Fig. 8a) and Ar atmospheres (Fig. 8b). When the impedance magnitude plot is independent of frequency and appears flat, this corresponds to low impedance phase angles. Such behavior is indicative of a film which behaves like a pure resistor with a minimal reactive component, while fast changing impedance magnitude or phase angle is representative of a capacitive or inductive response [25]. There is rich detail in the impedance spectra that show the differences between the responses of films annealed in air versus those annealed in Ar displayed in Fig. 8. Future publications will expound on these differences.,

For the purposes of this paper, the DC resistance of the films was estimated by averaging the impedance magnitude for frequencies less than 0.4 Hz, where the value of the impedance phase angle θ was sufficiently small and close to zero. For those highly insulating samples, for which the impedance phase angle did not reduce sufficiently close to zero at 0.4 Hz, the dc resistance was estimated by extrapolating the impedance magnitude to the frequency where the phase angle was extrapolated to zero. This approach was taken instead of extending impedance spectroscopy measurements to very low frequencies to allow the phase angle to approach zero. This was necessary because instrument limitations tended to make the extremely low frequency data too noisy to be useful. The variation of film resistivity with annealing temperature, calculated from the dc resistance obtained as described above, is presented in Fig. 9 for films annealed in air and in Ar. It can be seen that there was a substantial decrease in the film resistivity (from $>10^8$ Ω cm down to $<10^0$ Ω cm) with increased annealing temperature for films annealed in both air and Ar. It is important to note that the error bars shown in Fig. 9 are barely larger than the average data symbols, so the differences in resistivity observed can be said to be real experimental trends.

The defect structure of ITO has been studied and modeled by Frank and Köstlin [26], González et al. [26], and others [27–32]. Although indium oxide has a large band gap, ITO is a degenerate semiconductor because of tin doping. Tin forms Sn–O clusters of various co-ordinations on doping in In_2O_3. Of these, $(2Sn_{In}^{\cdot}O_i'')^{\times}$ is loosely bound, and can be reduced by removal of oxygen, which results in the release of mobile electrons as described the following defect equation:

$$2\left(2Sn_{In}^{\cdot}O_i''\right)^{\times} \rightarrow O_2(g) + 4Sn_{In}^{\cdot} + 4e'$$

Hence, it is expected that annealing in UHP Ar, where the partial pressure of oxygen is lower, will result in a higher carrier concentration, and hence a lower resistivity than films annealed in air. However, as shown in Figs. 8 and 9, annealing in air resulted in a more significant reduction in the impedance magnitude and the dc resistivity at lower temperature ($\sim$300 °C) than when annealing in Ar, which required 450 °C to show a significant decrease. Thus, additional changes in the microstructure, related to the removal of insulating phases and some degree of sintering must be the dominant factor in the reduction of film resistivity.

Discussion of results

Figure 10 depicts the expected microstructure of ITO colloidal films at different stages of the annealing treatment. The schematics were developed based on previously reported [15] AFM imaging and Scherrer analysis of X-ray scans in air annealed samples, which showed that the ITO particle size does not appear to change with increasing temperature. Similar data were obtained for Ar-annealed films but are not shown here for the sake of brevity. Instead, we present schematics that can more clearly depict what we expect is happening to the films during the annealing treatments since obtaining high resolution TEM images of the films to see the differences in the very fine nanoparticle interfaces (<1 nm) is beyond the scope of this paper.

Figure 10a shows a schematic of an as-deposited colloidal ITO film made from nanoparticles. It should be

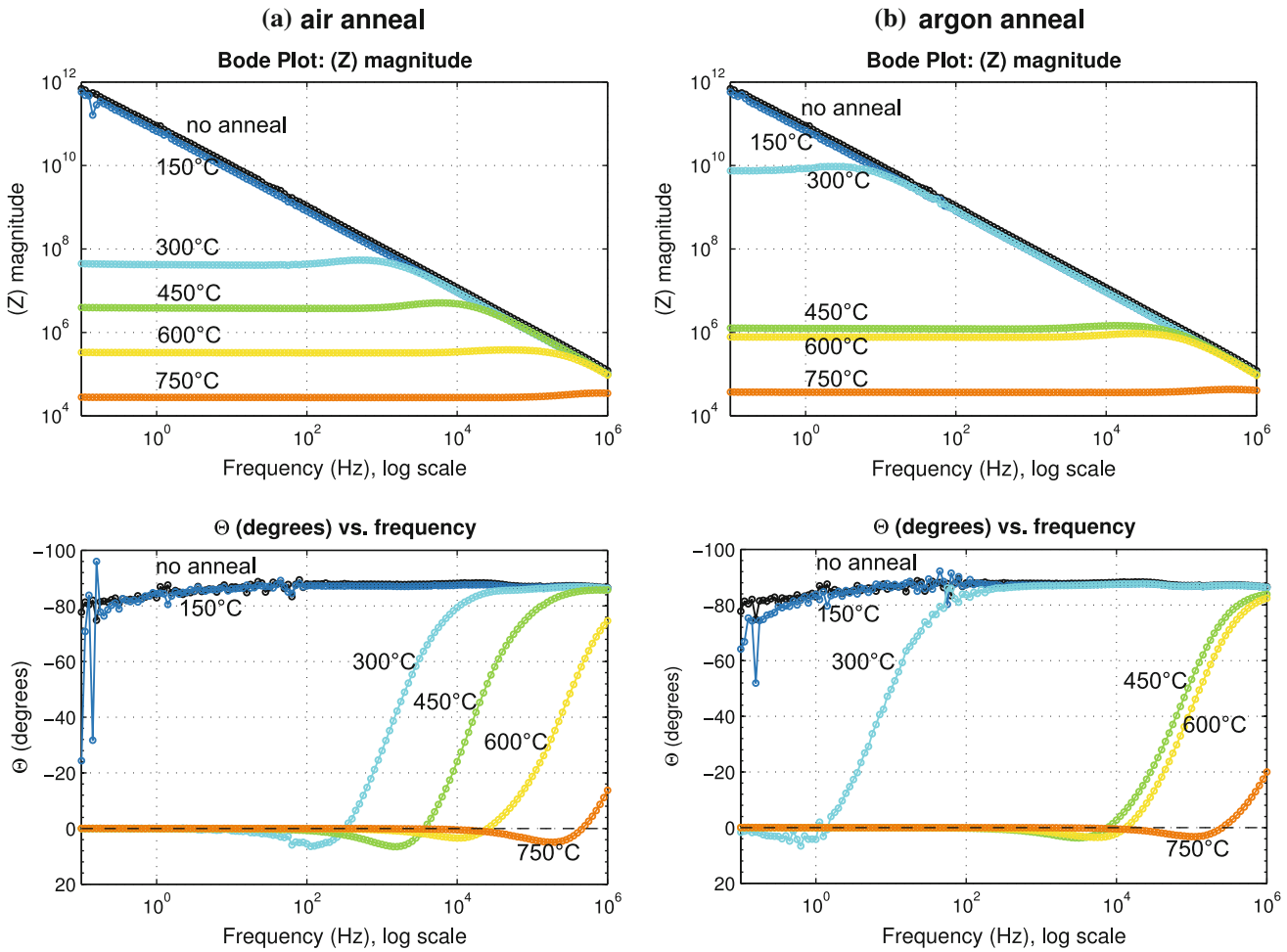

Fig. 8 Representative Bode plots showing a comparison of the impedance magnitude and phase angles for colloidal ITO films annealed at different temperatures in **a** air, **b** Ar

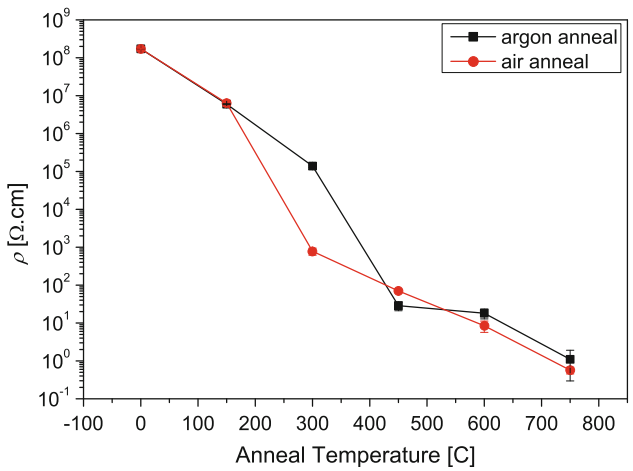

Fig. 9 DC resistivity of sputtered ITO films versus annealing temperature

mentioned that the schematics are not drawn to scale since the nanoparticles are expected to be ~6–8 nm in diameter while the organic coatings in the as-deposited film will be much less than 1 nm. The presence of insulating organics and voids in the ITO film suggests that the spin-coated ITO thin films can be considered as a composite consisting of conducting ITO nanoparticle islands embedded in an insulating phase of organics and voids. Annealing at a temperature that is less than the temperature needed for a complete removal of organics would naturally result in only a partial removal of the organics, at most. This is especially manifested in the colloidal films annealed in Ar at 300 °C. Raman characterization indicates the presence of significant amounts of amorphous carbon, which was likely produced as a result of incomplete pyrolysis of the organics. The resulting microstructure can be schematically represented by Fig. 10b, which shows some limited electrical contact between the nanoparticles, but at the same time, separation of the nanoparticles by an amorphous organic or a partially pyrolyzed carbonaceous phase. This microstructure not only results in high resistivity, but also a significantly reduced transmittance in the visible region. In comparison, the films annealed at 300 °C in air have a

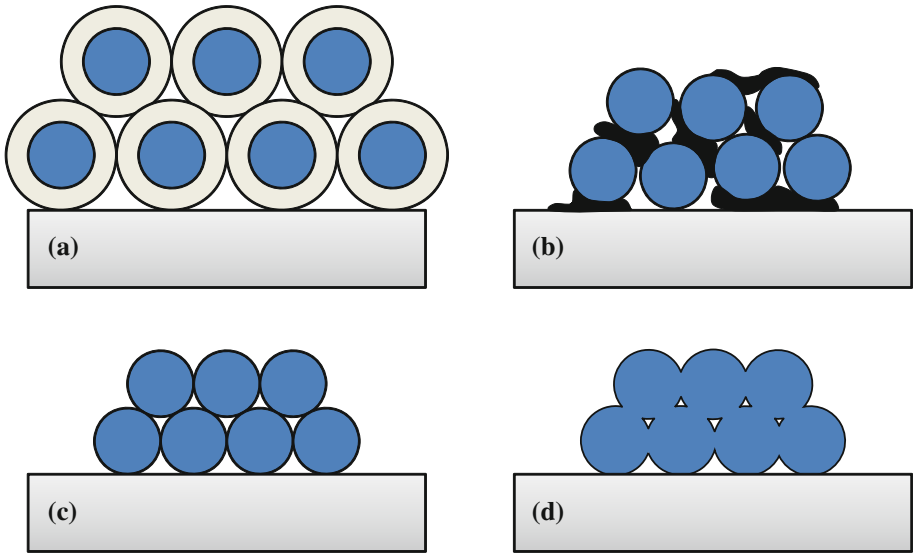

Fig. 10 Schematics of microstructural changes in ITO films made from ~ 6 nm colloidal ITO nanoparticles with increased annealing temperature (not drawn to scale): **a** colloidal ITO particles covered with passivating organics in the as-coated film, **b** colloidal particles with partially pyrolyzed organics, **c** colloidal particles with organics removed, **d** partially sintered colloidal particles

higher proportion of carbon removal, as evidenced from the TGA and Raman characterization. This resulted in the resistivity being more than 2–3 orders of magnitude lower than for films annealed at the same temperature in Ar (see Fig. 9).

As can be inferred from the TGA data, the removal of organic content increases with an increase in the annealing temperature, during annealing in either atmosphere. The removal of the organics and reduction of porosity through the densification process has the effect of increasing the proportion of the conducting phase in this "composite" film. Figure 10c shows a schematic of the expected microstructure of the colloidal film, when all or most of the organics would have been removed. In this case, the ITO nanoparticles would be in contact with each other, and this would result in a much lower resistivity than when organic phases are present in a significant proportion to hinder electrical transport. Although the ITO nanoparticles are in contact with each other, the resistivity of the film is not reduced all the way close to that of bulk ITO, which is $<10^{-3}$ Ω cm, presumably due to non-ideal contact as a result of the presence of remaining void space in between the ITO nanoparticles.

Low temperature annealing is expected to result in very little sintering between the nanoparticles resulting in a non-optimal contact between them. This is supported by the previously discussed Scherer analysis [15], which demonstrated that the nanoparticles do not change size at all in the temperature range studied, except for a minimal change for the 750 °C treatment. The nano-porosities that are present between the nanoparticles act as an insulating phase, and therefore limit the charge transfer between the conducting ITO nanoparticles. Annealing at higher temperatures would be expected to cause some densification resulting from necking between the particles. This is schematically represented in Fig. 10d. Thus, annealing at even higher temperatures would result in continued lowering of the resistivity due to increased densification of the nanoparticulate film.

As a result of all these factors, the resistivity versus annealing temperature curve shows several order of magnitude changes in resistivity over the temperature range studied, which are comparable to percolation curves as a function of the volume fraction of conductive phase in composites such as metal–polymer composites and others [33]. In fact, for both the air and Ar-annealed ITO spin-coated films, the lowest resistivity achieved was in the order of 10^0 Ω cm which was arrived at via oxidation and pyrolysis, respectively. This was supported by the Raman spectra and TGA which indicated that the removal of organics is more efficient at lower temperatures in the oxidative atmosphere of air as compared to the low oxygen partial pressure atmosphere of Ar. Although annealing in the low oxygen partial pressure of Ar might have marginally increased the carrier concentration by the process described earlier, the reduction of scattering as a result of removal of organics and partial densification has a far more dominant effect in reducing the resistivity of the colloidal ITO films.

In closing, this article has shown that the mechanism of organic removal, whether it is controlled by oxidation or pyrolysis, plays a crucial role in determining the electrical properties and the transparency of the colloidal ITO thin films described here. The authors have previously shown that plasma treatment can reduce the organics content in the films and can significantly decrease the resistivity even without any annealing [15]. It is suggested that optimized plasma annealing (high pressure reactive ion etching) in combination with low temperature annealing techniques such as flash lamp annealing, also referred to as

millisecond/microsecond annealing [34–36], pulsed-laser annealing [37–39] may help attain even lower resistivity values in colloidal ITO films fabricated this way.

Conclusions

Although ITO is a good electrical conductor, colloidal ITO films are very resistive in the as-deposited condition due to the lack of good inter-particle contact as a result of the presence of a coating of stabilizing organic phases that are very insulating. Annealing at a high temperature is the simplest way to decrease or remove these organics and also help induce coalescence and densification. It was shown that annealing at high temperatures can significantly decrease the resistivity of colloidal ITO thin films over several orders of magnitude by establishing electrical percolating paths between the nanoparticles and also by reducing electron scattering by inter-particle necking and densification. However, sufficiently low resistivity values to be practical for flexible electronic applications cannot easily be achieved by conventional low temperature annealing alone and other treatments must be considered.

Acknowledgments The authors would like to acknowledge and thank Joseph Dorsheimer and Alexander Rhzevskii of Thermo Scientific, Inc. for their help with Raman characterization of these films. Sarang Deodhar of Georgia Tech assisted with the TGA characterization. Funding from the Institute of Paper Science & Technology Alumni Association Scholarship Endowment Fund at Georgia Tech and partial support from the US Department of Energy under DE-FG 02-03-ER 46035 are acknowledged.

References

1. Hamberg I, Granqvist CG (1986) J Appl Phys 60(11):R123
2. Edwards PP, Porch A, Jones MO, Morgan DV, Perks RM (2004) Dalton Trans 19:2995. doi:10.1039/b408864f
3. Chopra KL, Major S, Pandya DK (1983) Thin Solid Films 102:1
4. Minami T, Kuboi T, Miyata T, Ohtani Y (2008) Phys Status Solidi A-Appl Mat 205(2):255. doi:10.1002/pssa.200622541
5. Gordon RG (2000) MRS Bull 25(8):52
6. Lewis BG, Paine DC (2000) MRS Bull 25(8):22
7. Shigesato Y, Paine DC (1993) Appl Phys Lett 62(11):1268
8. Izumi H, Ishihara T, Yoshioka H, Motoyama M (2002) Thin Solid Films 411(1):32
9. Hong HS, Jung H, Hong S-J (2010) Res Chem Intermed 36(6–7):761
10. Matthews S, De Bosscher W, Blondeel A, Van Holsbeke J, Delrue H (2008) Vacuum 83(3):518. doi:10.1016/j.vacuum.2008.04.065
11. Straue N, Rauscher M, Walther S, Faber H, Roosen A (2009) J Mater Sci 44(22):6011. doi:10.1007/s10853-009-3804-1
12. Yin Y, Zhou S, Gu G, Wu L (2007) J Mater Sci 42(15):5959. doi:10.1007/s10853-006-1133-1
13. Carotenuto G, Valente M, Sciume G, Valente T, Pepe G, Ruototo A, Nicolais L (2006) J Mater Sci 41(17):5587. doi:10.1007/s10853-006-0253-y
14. Capozzi CJ, Ivanov IN, Joshi S, Gerhardt RA (2009) Nanotechnology 20(14):145701
15. Joshi SM, Book GW, Gerhardt RA (2012) Thin Solid Films 520(7):2723. doi:10.1016/j.tsf.2011.11.052
16. Gehl B, Fromsdorf A, Aleksandrovic V, Schmidt T, Pretorius A, Flege JI, Bernstorff S, Rosenauer A, Falta J, Weller H, Baumer M (2008) Adv Funct Mater 18(16):2398
17. Robbins LA, Cusak RW (1997) In: Perry RH, Green DW (eds) Perry's chemical engineers' handbook, 7th edn. McGraw-Hill, New York, p 15.11
18. AIST:RIO-DB Spectral Database for Organic Compounds, SDBS. (2011) http://riodb01.ibase.aist.go.jp/sdbs/cgi-bin/cre_index.cgi
19. Sigma-Aldrich.com. http://www.sigmaaldrich.com
20. Plot Digitizer. http://plotdigitizer.sourceforge.net/
21. Smith E, Dent G (2006) Modern Raman spectroscopy: a practical approach. Wiley, West Sussex
22. 1-Octadecene (alpha-olefin C18) (2012) http://www.chemicalland21.com/industrialchem/organic/1-OCTADECENE.htm
23. Ferrari AC, Robertson J (2000) Phys Rev B 61(20):14095
24. Schwan J, Ulrich S, Batori V, Ehrhardt H, Silva SRP (1996) J Appl Phys 80(1):440. doi:10.1063/1.362745
25. Gerhardt RA (2005) In: Liedl G, Wyder P, Bassani G (eds) Encyclopedia of condensed matter physics. Elsevier, Oxford, p 350
26. Frank G, Köstlin H (1982) Appl Phys A 27(4):197
27. Gonzalez GB, Mason TO, Quintana JP, Warschkow O, Ellis DE, Hwang JH, Hodges JP, Jorgensen JD (2004) J Appl Phys 96(7):3912
28. Hamberg I, Granqvist CG, Berggren KF, Sernelius BE, Engström L (1984) Phys Rev B 30(6):3240
29. Nadaud N, Lequeux N, Nanot M, Jove J, Roisnel T (1998) J Solid State Chem 135(1):140
30. Warschkow O, Ellis DE, Gonzalez GB, Mason TO (2003) J Am Chem Soc 86(10):1700
31. Warschkow O, Ellis DE, Gonzalez GB, Mason TO (2003) J Am Chem Soc 86(10):1707
32. Warschkow O, Miljacic L, Ellis DE, Gonzalez G, Mason TO (2006) J Am Chem Soc 89(2):616
33. Sahimi M (1994) In: Applications of percolation theory. Taylor & Francis, London
34. Kim H-S, Dhage SR, Shim D-E, Hahn HT (2009) Appl Phys A 97(4):791
35. Schroder KA, McCool SC, Furlan WF (2006) In: 2006 NSTI nanotechnology conference and trade show, Boston, MA, 2006. NSTI Nanotech 2006 Technical Proceedings. Nano Science and Technology Institute, p 198
36. Ito T, Iinuma T, Murakoshi A, Akutsu H, Suguro K, Arikado T, Okumura K, Yoshioka M, Owada T, Imaoka Y, Murayama H, Kusuda T (2002) Jpn J Appl Phys Pt 1(41):2394
37. Delmdahl R, Fechner B (2010) Appl Phys A 101(2):283
38. Huang W, El-Sayed MA (2008) Eur Phys J Spec Top 153(1):223
39. Sameshima T (2009) Appl Phys A 96(1):137